OXFORD

Human Molecular Genetics, 2015, Vol. 24, No. 24 7017–7030

doi: 10.1093/hmg/ddv403
Advance Access Publication Date: 29 September 2015
Original Article

ORIGINAL ARTICLE

A study of whirlin isoforms in the mouse vestibular system suggests potential vestibular dysfunction in *DFNB31*-deficient patients

Pranav Dinesh Mathur[1,2], Sarath Vijayakumar[3], Deepti Vashist[1], Sherri M. Jones[3], Timothy A. Jones[3] and Jun Yang[1,2,4,*]

[1]Department of Ophthalmology and Visual Sciences, Moran Eye Center, University of Utah, 65 Mario Capecchi Drive, Salt Lake City, UT 84132, USA, [2]Department of Neurobiology and Anatomy, University of Utah, 20 North 1900 East, Salt Lake City, UT 84132, USA, [3]Department of Special Education and Communication Disorders, University of Nebraska-Lincoln, 304 Barkley Memorial Center, Lincoln, NE 68583, USA and [4]Division of Otolaryngology, Department of Surgery, University of Utah, 50 North Medical Drive, Salt Lake City, UT 84132, USA

*To whom correspondence should be addressed at: John A Moran Eye Center, University of Utah, 65 Mario Capecchi Drive, Bldg 523, Salt Lake City, UT 84132, USA. Tel: +1 801 213 2591; Email: jun.yang@hsc.utah.edu

Abstract

The *DFNB31* gene plays an indispensable role in the cochlea and retina. Mutations in this gene disrupt its various isoforms and lead to non-syndromic deafness, blindness and deaf-blindness. However, the known expression of *Dfnb31*, the mouse ortholog of *DFNB31*, in vestibular organs and the potential vestibular-deficient phenotype observed in one *Dfnb31* mutant mouse (*Dfnb31*$^{wi/wi}$) suggest that *DFNB31* may also be important for vestibular function. In this study, we find that full-length (FL-) and C-terminal (C-) whirlin isoforms are expressed in the vestibular organs, where their stereociliary localizations are similar to those of developing cochlear inner hair cells. No whirlin is detected in *Dfnb31*$^{wi/wi}$ vestibular organs, while only C-whirlin is expressed in *Dfnb31*$^{neo/neo}$ vestibular organs. Both FL- and C-whirlin isoforms are required for normal vestibular stereociliary growth, although they may play slightly different roles in the central and peripheral zones of the crista ampullaris. Vestibular sensory-evoked potentials demonstrate severe to profound vestibular deficits in *Dfnb31*$^{neo/neo}$ and *Dfnb31*$^{wi/wi}$ mice. Swimming and rotarod tests demonstrate that the two *Dfnb31* mutants have balance problems, with *Dfnb31*$^{wi/wi}$ mice being more affected than *Dfnb31*$^{neo/neo}$ mice. Because *Dfnb31*$^{wi/wi}$ and *Dfnb31*$^{neo/neo}$ mice faithfully recapitulate hearing and vision symptoms in patients, our findings of vestibular dysfunction in these *Dfnb31* mutants raise the question of whether *DFNB31*-deficient patients may acquire vestibular as well as hearing and vision loss.

Introduction

DFNB31 is the causative gene for Usher syndrome type 2 USH2D (OMIM; 611383) (1–3) and non-syndromic deafness DFNB31 (OMIM; 607084) (4,5) with USH2D being characterized by moderate to severe hearing loss and progressive retinal degeneration. A recent study also identified a *DFNB31* mutation in patients with only progressive retinal degeneration (6). These phenotypes of hearing loss and retinal degeneration are recapitulated in mice carrying a mutant *Dfnb31* gene, the ortholog of *DFNB31* and also known as *Whrn* (7). Therefore, *DFNB31*/*Dfnb31* is essential for both hearing and vision. *Dfnb31* expresses multiple whirlin isoforms in cochlear hair cells and retinal photoreceptors (8–10). In the cochlea, full-length (FL-) whirlin isoform is localized at stereociliary tips and ankle link complexes in inner hair cells

Received: July 22, 2015. **Revised:** September 10, 2015. **Accepted:** September 21, 2015

and stereociliary ankle link complexes in outer hair cells; C-terminal (C-) whirlin isoform is present at stereociliary tips in both inner and outer hair cells. The FL- and C-whirlin isoforms at hair cell stereociliary tips are required for normal stereociliary elongation (4,10,11), while FL-whirlin isoform also participates in the formation of the ankle link complex (12,13), which is a transient subcellular structure during cochlear stereociliary bundle development (14–16). Defects in the ankle link complex are associated with Usher syndrome type 2 (USH2) (13,16) (manuscript submitted). In photoreceptors, FL- and probably N-terminal (N-) whirlin isoforms organize the formation of the periciliary membrane complex between the outer and inner segment (10). Although the function of the periciliary membrane complex is currently unclear, defects in this structure are known to cause retinal degeneration (7). Our previous study demonstrates that the differential expression, localization and function of various whirlin isoforms underlie the distinct phenotypical combinations in mice carrying different *Dfnb31* mutations (10) and are highly likely the cause of variable disease manifestations of *DFNB31* mutations in humans.

In addition to its cochlear and retinal expressions, *Dfnb31* has been reported to have nine mRNA variants and its protein isoforms were localized at hair cell stereociliary tips and ankle link complexes in mouse and rat vestibular systems (9,15,17,18). Furthermore, *Dfnb31*$^{wi/wi}$ mice with a deletion between *Dfnb31* exons 6 and 9 (Fig. 1A) exhibit circling and head-bobbing behaviors (4,19), suggestive of vestibular dysfunction. In contrast, *Dfnb31*$^{neo/neo}$ mice with a mutation in *Dfnb31* exon 1 show no overt balance disorder phenotype. Therefore, it is important to understand the role of whirlin isoforms in the vestibular system. In this study, we thoroughly investigated whirlin isoforms in mouse vestibular end organs. We found that the expression, localization and function of whirlin isoforms in vestibular hair cells (VHCs) are similar to those of developing cochlear inner hair cells. Examinations of stereociliary morphology, vestibular function and balance behaviors clearly demonstrated the existence of peripheral vestibular dysfunction in *Dfnb31*$^{neo/neo}$ and *Dfnb31*$^{wi/wi}$ mice, which are USH2D and DFNB31 animal models, respectively. Therefore, our findings prompt the question of whether *DFNB31*-deficient patients harbor occult peripheral vestibulopathy.

Results

Expression and localization of whirlin isoforms in the wild-type, *Dfnb31*$^{neo/neo}$ and *Dfnb31*$^{wi/wi}$ vestibular systems

Eleven *Dfnb31* mRNA variants identified previously from the mouse inner ear and retina (8,17) were investigated in the

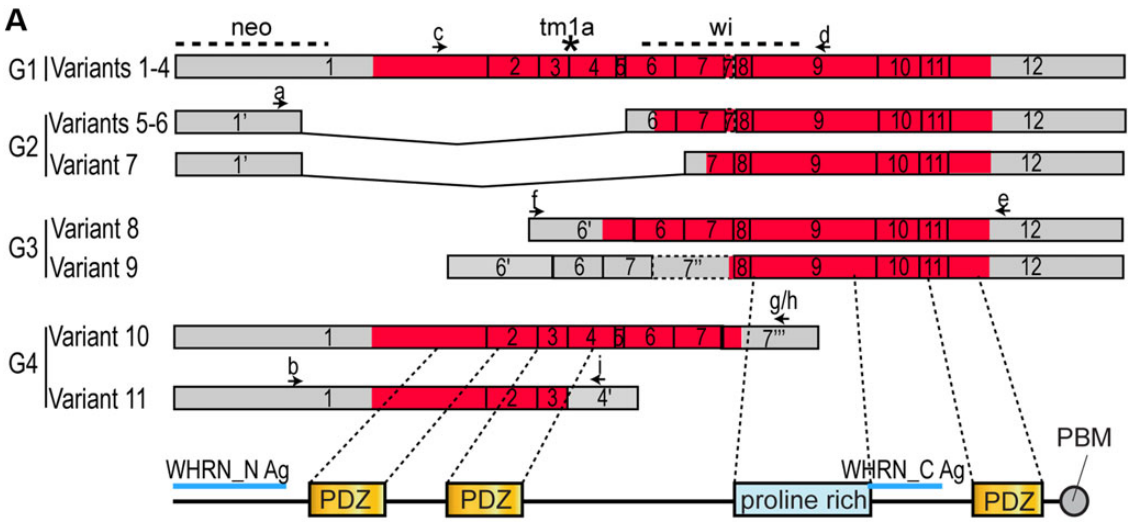

B

Protein isoform		FL-whirlin	C-whirlin			N-whirlin	
Variant groups		Group 1	Group 2	Group 3		Group 4	
Variants		Variants 1-4	Variants 5-7	Variant 8	Variant 9	Variant 10	Variant 11
GenBank Accession #		AY739114-AY739117	AY739118-AY739120	AY739121	AY739122	AK157955 HQ148552	HQ148553
Primer pairs		c/d	a/d	f/e	f/e	c/g or c/h	b/i
Vestibular System	wt	+	-	+	-	-	-
	neo	-	-	+	-	-	-
	wi	T	-	T	-	-	-

Figure 1. Expression of *Dfnb31* mRNA variants in wild-type and *Dfnb31* mutant vestibular systems. (**A**) Schematic diagram of various *Dfnb31* mRNA variants identified previously from the mouse inner ear and retina (8,17). Arabic numerals are exon numbers. Gray and red colors indicate untranslated and protein coding regions, respectively. Arrows and lower case letters show the position and direction of primers used for RT–PCR experiments in (**B**). Positions of *Dfnb31*$^{neo/neo}$, *Dfnb31*$^{wi/wi}$ and *Dfnb31*$^{tm1a/tm1a}$ mutations are labeled by dashed lines and an asterisk at the top. The exon regions corresponding to whirlin protein functional domains are shown at the bottom. Blue lines indicate the antigen regions of whirlin antibodies. (B) Summary of RT–PCR results showing differential disruption of *Dfnb31* mRNA variants in *Dfnb31*$^{neo/neo}$ (neo) and *Dfnb31*$^{wi/wi}$ (wi) vestibular systems. In general, variant 8 was intact, while variants 1–4 were disrupted in the *Dfnb31*$^{neo/neo}$ vestibular system; variants 1–4 and 8 were all truncated in the *Dfnb31*$^{wi/wi}$ vestibular system. +, presence; –, absence; T, truncated.

mouse vestibular system in this study. These *Dfnb31* mRNA variants were categorized into four groups according to their alternative use of promoters and alternative splicing of exons (Fig. 1A). Variants of Group 1 can be translated into FL-whirlin possessing three PDZ domains and one proline-rich region. Group 2 variants share the same promoter region with Group 1, but are alternatively spliced to skip regions between exons 1–5 and exons 1–6, while Group 3 variants utilize alternative promoters in intron 5. The variants in Groups 2 and 3 are predicted to be translated into proteins with only the proline-rich region and the third PDZ domain (C-whirlin). Variants in Group 4 undergo alternative splicing after exon 4 or 7, which leads to protein isoforms with only N-terminal one or two PDZ domains (N-whirlin). We designed primers specific to each group of *Dfnb31* mRNA variants (Fig. 1A and Supplementary Material, Table S1) and characterized the expression of these *Dfnb31* variants by RT–PCR using total RNA isolated from combined P4 mouse saccules, utricles and cristae. In the wild-type vestibular system, variants in Group 1 as well as variant 8 in Group 3 were expressed (Fig. 1B). In the *Dfnb31*$^{neo/neo}$ vestibular system, which carries the *Dfnb31* mutation in the 5′ region of exon 1 (Fig. 1A), variant 8 was intact, while others were undetectable (Fig. 1B). Finally, the *Dfnb31*$^{wi/wi}$ mutation (Fig. 1A) produced truncated Group 1 variants and variant 8 in the vestibular system (Fig. 1B), which results in frameshift and premature termination of their protein translation. The truncated Group 1 protein products have amino acid sequences similar to N-whirlin followed by 58 aberrant amino acids from the out-of-frame sequence, while the truncated variant 8 protein product has 76 whirlin amino acids with no known functional domains as well as the 58 aberrant amino acids.

The above RT–PCR results suggested that FL- and C-whirlins existed in the wild-type vestibular system, C-whirlin in the *Dfnb31*$^{neo/neo}$ vestibular system, and truncated N-whirlin in the *Dfnb31*$^{wi/wi}$ vestibular system. To reveal the subcellular locations of these whirlin isoforms in VHCs, we performed immunostaining of mouse vestibular whole-mounts at P4 using rabbit WHRN_N and WHRN_C antibodies, which specifically detect against the whirlin N- and C-terminal regions, respectively (Fig. 1A and data not shown). Immunoreactivities of WHRN_C were found at the tips of the tallest stereocilia and bases of probably all stereocilia in wild-type VHCs (Fig. 2Aa–Ab), at only the tips of the tallest stereocilia in *Dfnb31*$^{neo/neo}$ VHCs (Fig. 2Ac–Ae), and absent in *Dfnb31*$^{wi/wi}$ VHCs (Fig. 2Ae). Additionally, immunoreactivities of WHRN_N were found in regions similar to those of WHRN_C in wild-type VHCs (Fig. 2B) and absent in *Dfnb31*$^{neo/neo}$ and *Dfnb31*$^{wi/wi}$ VHCs (data not shown). Therefore, FL-whirlin is present at both stereociliary tips and ankle link complexes, and C-whirlin is only at stereociliary tips in wild-type VHCs. In *Dfnb31*$^{neo/neo}$ VHCs, C-whirlin is at stereociliary tips. The truncated N-whirlin may not exist in *Dfnb31*$^{wi/wi}$ VHCs due to nonsense-mediated mRNA decay.

Stereociliary morphology, cytocauds and hair cell density in *Dfnb31*$^{neo/neo}$ and *Dfnb31*$^{wi/wi}$ vestibular systems

The vestibular system consists of the otolith organs (saccule and utricle) and semicircular canals (crista ampullaris). We examined the VHC stereociliary morphology of *Dfnb31*$^{neo/neo}$ and *Dfnb31*$^{wi/wi}$ mice by phalloidin staining of saccules, utricles and cristae at P4. We utilized oncomodulin, calretinin and β-III tubulin as markers

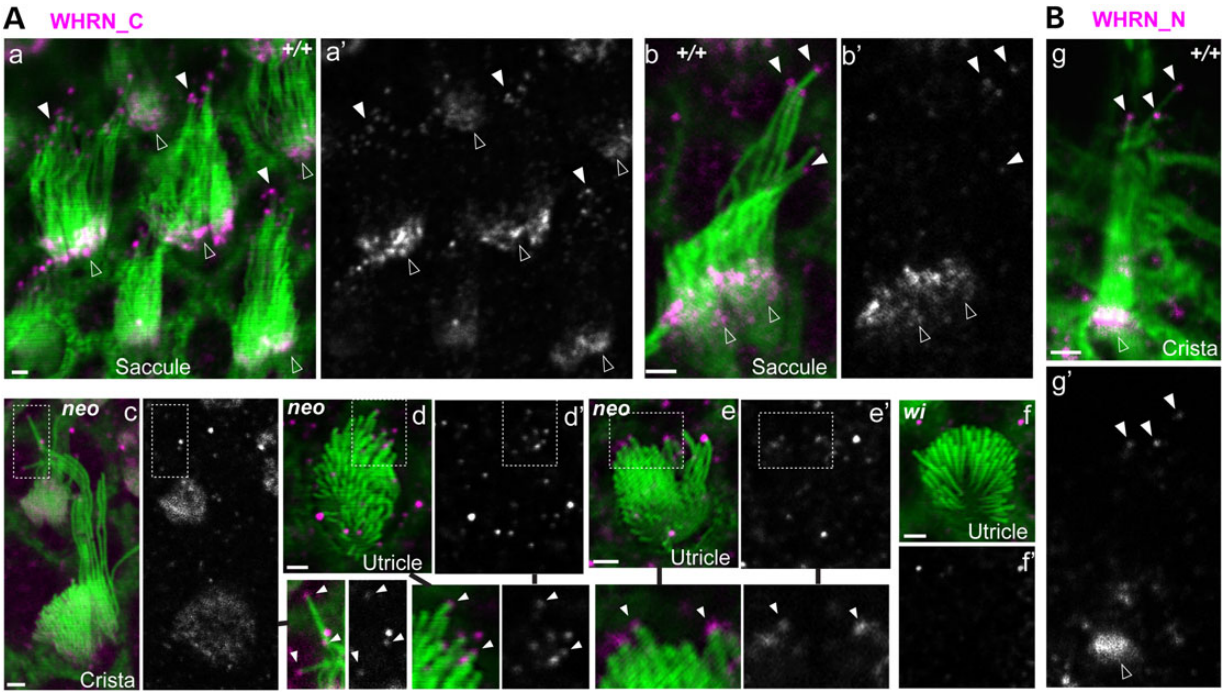

Figure 2. Whirlin protein localization in wild-type, *Dfnb31*$^{neo/neo}$ and *Dfnb31*$^{wi/wi}$ VHCs. (**A**) Immunostaining using rabbit WHRN_C antibody showed signals at stereociliary bases and tips in wild-type VHCs (+/+, **a** and **b**), signals at stereociliary tips in *Dfnb31*$^{neo/neo}$ VHCs (*neo*, **c–e**) and no stereociliary signals in *Dfnb31*$^{wi/wi}$ VHCs (*wi*, **f**) at P4. Note weak diffuse whirlin signals were also found in the cuticular plate of VHCs in the *Dfnb31*$^{neo/neo}$ peripheral crista (c). Signals from the magenta channel are shown in grayscale (**a′–f′**) on the right of the merged images (a–f). Regions in the dashed frames are enlarged either on the right of (c, and c′) or below (d, d′, c and c′) the original images and are linked by black lines. (**B**) Immunostaining using rabbit WHRN_N antibody showed signals at stereociliary bases and tips in P4 wild-type VHCs. Signals from the magenta channel are shown in grayscale (g′) below the merged image (g). Green, phalloidin; magenta, whirlin signals. Some magenta signals on or outside stereociliary bundles are non-specific. Scale bars, 1 μm.

to distinguish VHCs of the macular striola and extrastriola, VHCs of the crista central and peripheral regions as well as type I and type II VHCs. Oncomodulin is expressed in type I hair cells of the macular striola and the crista central region, which accounts for the majority of VHCs in these regions (20). Calretinin mainly labels the calyceal afferent of type I cells (21,22) and the soma of type II cells (22,23) and thus gives empty circular and filled spot signal patterns, respectively. Additionally, β-III tubulin is a marker for type I calyceal afferents (22). Therefore, combined staining for calretinin and β-III tubulin gives circular signals surrounding phalloidin signals for type I cells mainly in the macular striola and the crista central region and filled spot signals for type II cells mainly in the macular extrastriola and the crista peripheral region. We found shortening of stereocilia throughout the entire saccule and utricle of both *Dfnb31*$^{neo/neo}$ and *Dfnb31*$^{wi/wi}$ mice (data not shown). However, stereocilia were short throughout the *Dfnb31*$^{wi/wi}$ crista, but only restricted to the central region of *Dfnb31*$^{neo/neo}$ cristae (Figs 2Ac, 3A and B and 4). Measurement of type I stereociliary length in the whole saccule and central crista stained by phalloidin at P4 and P30–40 demonstrated that *Dfnb31*$^{neo/neo}$ stereocilia were longer than *Dfnb31*$^{wi/wi}$ stereocilia, although both mutants were much shorter than wild-type stereocilia (Fig. 4). A careful examination revealed that *Dfnb31*$^{neo/neo}$ vestibular stereociliary bundles had a greater staircase spacing than *Dfnb31*$^{wi/wi}$ vestibular stereociliary bundles. We also compared the stereociliary length between type I and type II hair cells in the two whirlin mutant mice (Fig. 3C). We observed shorter type II stereocilia than type I stereocilia in both whirlin mutants. For example, in *Dfnb31*$^{neo/neo}$ central cristae, the stereociliary length of type I cells is 4.05 ± 0.24 μm (mean ± SE, $n = 36$ type I cells, 4 mice), and the stereociliary length of type II cells is 3.09 ± 0.15 μm (mean ± SE, $n = 34$ type II cells, 4 mice). Considering that type II stereocilia are ∼50% of type I stereocilia in length in the wild-type mouse utricle (22), the mutations in the two *Dfnb31* mutant mice probably affected both types of hair cells similarly.

To corroborate our observations from the phalloidin-stained vestibular whole mounts, we performed scanning electron microscopy (SEM) on wild-type, *Dfnb31*$^{neo/neo}$ and *Dfnb31*$^{wi/wi}$ otolith organs at P40–P45. Consistently, we observed shortened stereocilia throughout the entire utricle and saccule of the two *Dfnb31* mutants with *Dfnb31*$^{wi/wi}$ stereocilia being the shortest (Fig. 5A). Additionally, the stereocilia in both *Dfnb31*$^{neo/neo}$ and *Dfnb31*$^{wi/wi}$ VHCs were thicker relative to wild-type stereocilia, while the difference in thicknesses between *Dfnb31*$^{neo/neo}$ and *Dfnb31*$^{wi/wi}$ stereocilia was not statistically significant (Fig. 5B). This thick stereocilia phenotype was also reported previously in *Dfnb31*$^{neo/neo}$ and *Dfnb31*$^{wi/wi}$ cochlear hair cells (24,25). The high-magnification SEM images further allowed us to examine the staircase arrangement of *Dfnb31* mutant vestibular bundles by measuring the length difference (the spacing) between different stereociliary rows. In *Dfnb31*$^{neo/neo}$ vestibular bundles, we found that the spacing between the tallest and the second tallest stereociliary rows and the spacing between the second and third tallest stereociliary rows were significantly reduced by 47.75 and 61.30%, respectively (Fig. 5B). Because the longest stereocilia were shortened by 48.44%, as shown in P30–P40 *Dfnb31*$^{neo/neo}$ saccules (Fig. 4), this finding indicated that the tallest and second tallest stereociliary rows were shortened to a similar extent, while the third tallest stereociliary row was shortened more severely. Therefore, the staircase stereociliary arrangement in *Dfnb31*$^{neo/neo}$ VHCs was not affected significantly. In *Dfnb31*$^{wi/wi}$ otolith organs, hair bundles with two different abnormal morphologies were observed, wi1 and wi2 (labeled 1 and 2 in Fig. 5A, respectively). While both wi1 and wi2 bundles showed short stereocilia with similar length, wi1 bundles also had several taller stereocilia (arrows in Fig. 5A). Compared with wild-type vestibular bundles, the spacing between the tallest and second tallest rows and the spacing between the second and third tallest rows were reduced by 48.88 and 74.00% for wi1 bundles, respectively, and by 82.85 and 82.37% for wi2 bundles, respectively (Fig. 5B). Although not measured, the spacing between the third and the rest rows in wi1 bundles seemed similar to the spacing between rows in wi2 bundles (Fig. 5A). Therefore, both wi1 and wi2 bundles lacked the evident staircase stereociliary arrangement (Fig. 5A and B), although the remnant staircase pattern existed in wi1 bundles. These two *Dfnb31*$^{wi/wi}$ bundle morphologies might result from the difference between vestibular type I and type II cells, but further studies were needed to confirm this notion.

Cytocauds are a pathological structure of actin bundles commonly found in hair cells with abnormal stereociliary dimensions, such as *Dfnb31*$^{wi/wi}$ VHCs (26–31). Consistently, we found a large number of cytocauds in P4 *Dfnb31*$^{wi/wi}$ vestibular organs by phalloidin staining (Fig. 6A). This phenotype was also seen in P4 *Dfnb31*$^{neo/neo}$ vestibular organs (Fig. 6A). Three-dimensional (3D) reconstruction of z-stacked phalloidin-stained images clearly showed that cytocauds originated at the cuticular plate level and extended toward the cell body (Fig. 6B). From the top view, cytocauds appeared to originate from actin filaments close to the plasma membrane (magenta arrows in Fig. 6A). Additionally, measurement of hair cell numbers in the saccular striola showed that hair cell densities in the vestibular organs of the two whirlin mutants were comparable with those of wild-types at P30 (Fig. 6C).

Vestibular function of *Dfnb31*$^{neo/neo}$ and *Dfnb31*$^{wi/wi}$ mice

Vestibular function was directly assessed in adult mice (P30–P60) by linear vestibular sensory-evoked potential (VsEP) tests. Figure 7A illustrates vestibular response waveforms from representative wild-type, *Dfnb31*$^{neo/neo}$ and *Dfnb31*$^{wi/wi}$ mice. The VsEP waveforms reflect the vestibular macular response to the maximum stimulus level used in the present study (+6dB$_{re:1g/ms}$). Wild-type animals demonstrated typical VsEP responses comparable with standard control C57Bl/6J mice. In contrast, VsEP responses for the two whirlin mutant groups (*Dfnb31*$^{neo/neo}$ and *Dfnb31*$^{wi/wi}$) were either absent or they reflected mere remnants of a response. In both whirlin mutant groups, the results indicated a severe to profound loss of saccular and utricular function. VsEP was also examined in a third *Dfnb31* mutant mouse line, *Dfnb31*$^{tm1a/tm1a}$ (EUCOMM), which has a gene trap cassette after exon 3 (Fig. 1A) and has a disrupted whirlin isoform expression in the cochlea similar to that in the *Dfnb31*$^{neo/neo}$ cochlea (10). VsEP results in *Dfnb31*$^{tm1a/tm1a}$ mutants were comparable with those of *Dfnb31*$^{neo/neo}$ (data not shown).

Nine of the 14 *Dfnb31*$^{neo/neo}$ mice had no response at the highest stimulus levels (e.g. Fig. 7A), whereas responses were absent in 6 of the 12 *Dfnb31*$^{wi/wi}$ mice. The distributions were not significantly different. When present, vestibular responses of *Dfnb31*$^{neo/neo}$ and *Dfnb31*$^{wi/wi}$ mice were comparable. Among the 11 of 26 animals that had responses, VsEP thresholds (Fig. 7B), amplitudes (Fig. 7C, p1–n1, +6dB$_{re:1g/ms}$) and onset latencies (Fig. 7D, p1 latency, +6dBr:1g/ms) were not significantly different for the two mutant strains. One exception was that n1 latencies for *Dfnb31*$^{neo/neo}$ were slightly longer than those for *Dfnb31*$^{wi/wi}$ [Fig. 7D, multivariate analysis of variance (MANOVA), n1, least significant difference (LSD): $P = 0.05$, +6dB$_{re:1g/ms}$].

Of those mutant mice that had responses, thresholds for vestibular responses were significantly higher than wild-type

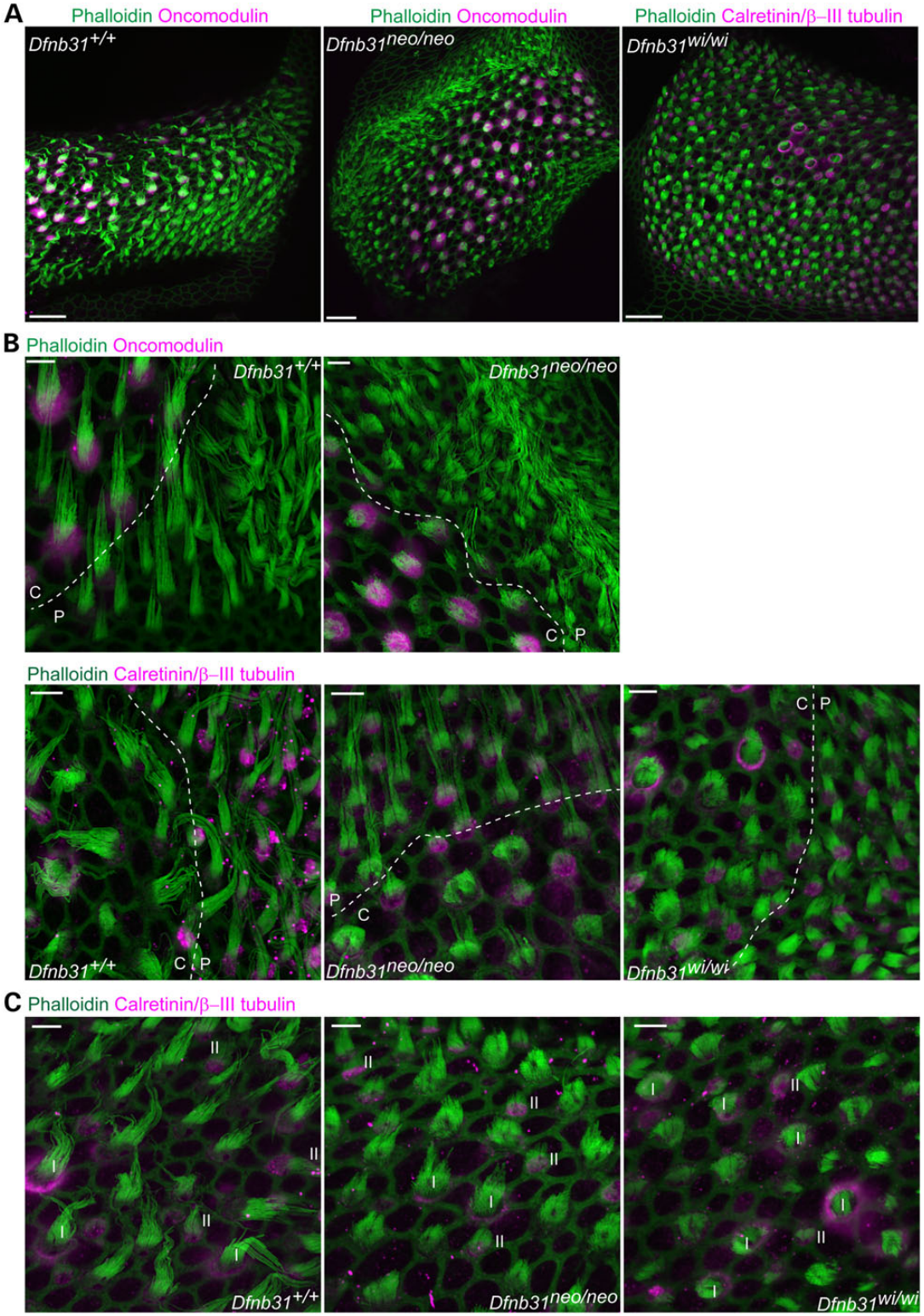

Figure 3. Stereociliary length is differentially affected in the central and peripheral regions of *Dfnb31*$^{neo/neo}$ but not *Dfnb31*$^{wi/wi}$ cristae. (**A**) Compared with stereociliary bundles of wild-type cristae (phalloidin, green), *Dfnb31*$^{neo/neo}$ stereociliary bundles were short in the central (oncomodulin positive, magenta) but not peripheral (oncomodulin negative) crista and *Dfnb31*$^{wi/wi}$ stereociliary bundles were short throughout the entire crista. Note that the central and peripheral region of *Dfnb31*$^{wi/wi}$ cristae were determined using the combined calretinin and β-III tubulin signals (magenta). Calyceal afferents (magenta circles) around stereociliary bundles are characteristic of type I hair cells in the central region. The images were taken at P4. (**B**) High-magnification images showing hair cell stereociliary bundles around the boundary (dashed lines) between the central (C) and peripheral (P) regions of P4 cristae. Upper row: central regions were labeled by oncomodulin staining. Lower row: central regions were determined by having type I hair cells (labeled as magenta circles) and wide shape of stereociliary bundles. (**C**) Both type I and type II stereociliary bundles were shortened in P4 *Dfnb31*$^{neo/neo}$ and *Dfnb31*$^{wi/wi}$ cristae. Type I (white Is) and type II (white IIs) hair cells were distinguished by combined calretinin and β-III tubulin signals (magenta circles, type I; magenta spots, type II). Scale bars, 20 μm in A and 5 μm in B and C.

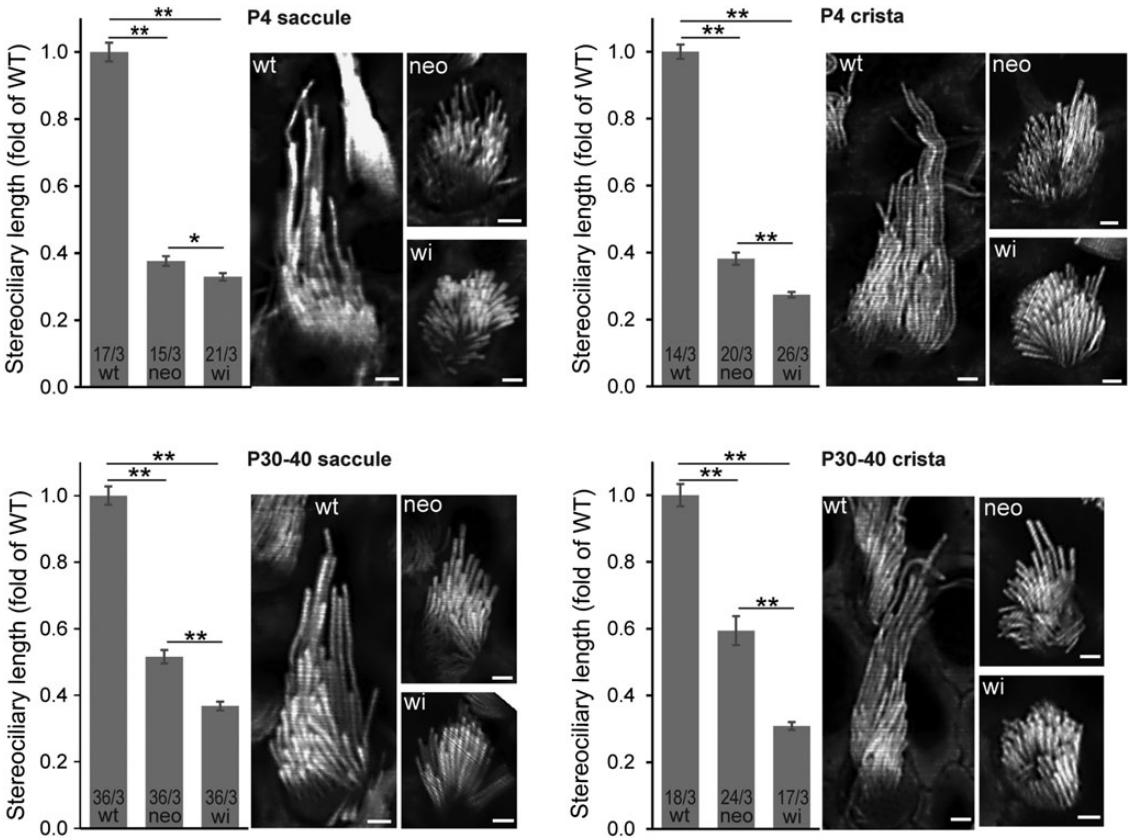

Figure 4. Stereociliary length and staircase arrangement in *Dfnb31*$^{neo/neo}$ and *Dfnb31*$^{wi/wi}$ vestibular hair bundles. Stereociliary length was measured in images captured from phalloidin-stained saccules (left) and cristae (right) at P4 (upper) and P30–40 (low). The stereocilia in both *Dfnb31*$^{neo/neo}$ (neo) and *Dfnb31*$^{wi/wi}$ (wi) vestibular systems were significantly shorter than those in wild-type vestibular system (wt). *Dfnb31*$^{wi/wi}$ vestibular stereocilia were even shorter than *Dfnb31*$^{neo/neo}$ vestibular stereocilia. Student's *t*-tests (two-tail) were performed. Numbers before and after slashes at the bottom of bar charts are the numbers of cells and animals analyzed, respectively. Compared with wild-type and *Dfnb31*$^{neo/neo}$ vestibular hair bundles, *Dfnb31*$^{wi/wi}$ vestibular hair bundles had less obvious staircase arrangement of stereocilia. Error bars, standard error of the mean; $^{**}P < 0.01$; scale bars, 1 μm.

(Fig. 7B; ANOVA, LSD; *Dfnb31*$^{neo/neo}$: $P = 1.0 \times 10^{-5}$; *Dfnb31*$^{wi/wi}$: $P = 4.3 \times 10^{-5}$, Table 1). Similarly, amplitudes were significantly lower (Fig. 7C, p1–n1, +6dB$_{re:1g/ms}$; ANOVA, *Dfnb31*$^{neo/neo}$: $P = 0.01$; *Dfnb31*$^{wi/wi}$: $P = 0.01$) and latencies significantly prolonged in mutant mice compared with wild-type animals (Fig. 7D; + 6dB$_{re:1g/ms}$, MANOVA, p1: *Dfnb31*$^{neo/neo}$: $P = 1.0 \times 10^{-7}$; *Dfnb31*$^{wi/wi}$: $P = 5.6 \times 10^{-7}$; n1: *Dfnb31*$^{neo/neo}$: $P = 2.0 \times 10^{-8}$; *Dfnb31*$^{wi/wi}$: $P = 2.2 \times 10^{-7}$; Table 1).

Despite the presence of responses in some mutant animals, the features of the responses reflected highly unusual characteristics (quantitative metrics are summarized in Table 1). Responses bore little resemblance to normal VsEPs. As noted above, response onset latencies were substantially delayed (>2 ms), amplitudes were considerably reduced. In addition, the relationship between latency and stimulus level was, depending on the animal, flat, degraded or, surprisingly, inverted (e.g. latency decreased with decreasing stimulus level). Figure 7C and D illustrates the mean amplitudes and latencies as a function of stimulus level for wild-type, *Dfnb31*$^{neo/neo}$ and *Dfnb31*$^{wi/wi}$ mice. The results for wild-type animals demonstrated the normal systematic increase in amplitudes and decrease in latencies as stimulus level is increased over a wide dynamic range. In contrast, the dynamic range for the responses of the *Dfnb31*$^{neo/neo}$ and *Dfnb31*$^{wi/wi}$ mice was very narrow (reflecting the high thresholds), and on average, latencies and amplitudes changed relatively little with increases in stimulus level (Fig. 7C and D).

Balance behaviors of *Dfnb31*$^{neo/neo}$, *Dfnb31*$^{wi/wi}$ and *Dfnb31*$^{wi/neo}$ mice

We evaluated balance behaviors of *Dfnb31*$^{neo/neo}$, *Dfnb31*$^{wi/wi}$ and *Dfnb31*$^{wi/neo}$ mice using swimming and rotarod tests. Although *Dfnb31*$^{neo/neo}$ and *Dfnb31*$^{wi/neo}$ mice did not show a circling behavior in the cage, they did exhibit irregular swimming behaviors including swimming in a circle and occasional immobile floating. However, *Dfnb31*$^{neo/neo}$ and *Dfnb31*$^{wi/neo}$ mice swam better than *Dfnb31*$^{wi/wi}$ mice, which mostly displayed underwater tumbling (Fig. 8A). A swimming test was also conducted for *Dfnb31*$^{tm1a/tm1a}$ mice, which did not exhibit circling and head-bobbing behaviors. Swimming results of *Dfnb31*$^{tm1a/tm1a}$ mutants were comparable with those of *Dfnb31*$^{neo/neo}$ mutants (data not shown). In the rotarod test, *Dfnb31*$^{neo/neo}$ and *Dfnb31*$^{wi/neo}$ mice were able to stay on the rotating rod longer than *Dfnb31*$^{wi/wi}$ mice but shorter than wild-type mice (Fig. 8B). Additionally, the performance of *Dfnb31*$^{wi/neo}$ mice in the swimming and rotarod tests was similar to *Dfnb31*$^{neo/neo}$ mice (Fig. 8A and B), indicating that the truncated N-whirlin from the *Dfnb31*^{wi} allele plays a negligible role in balance maintenance, consistent with our immunostaining finding that truncated N-whirlin may not exist at the protein level in *Dfnb31*$^{wi/wi}$ VHCs. In summary, the swimming and rotarod tests demonstrate that all tested *Dfnb31* mutant mice have some level of balance problems with the *Dfnb31*$^{wi/wi}$ mice having the worst balance performance.

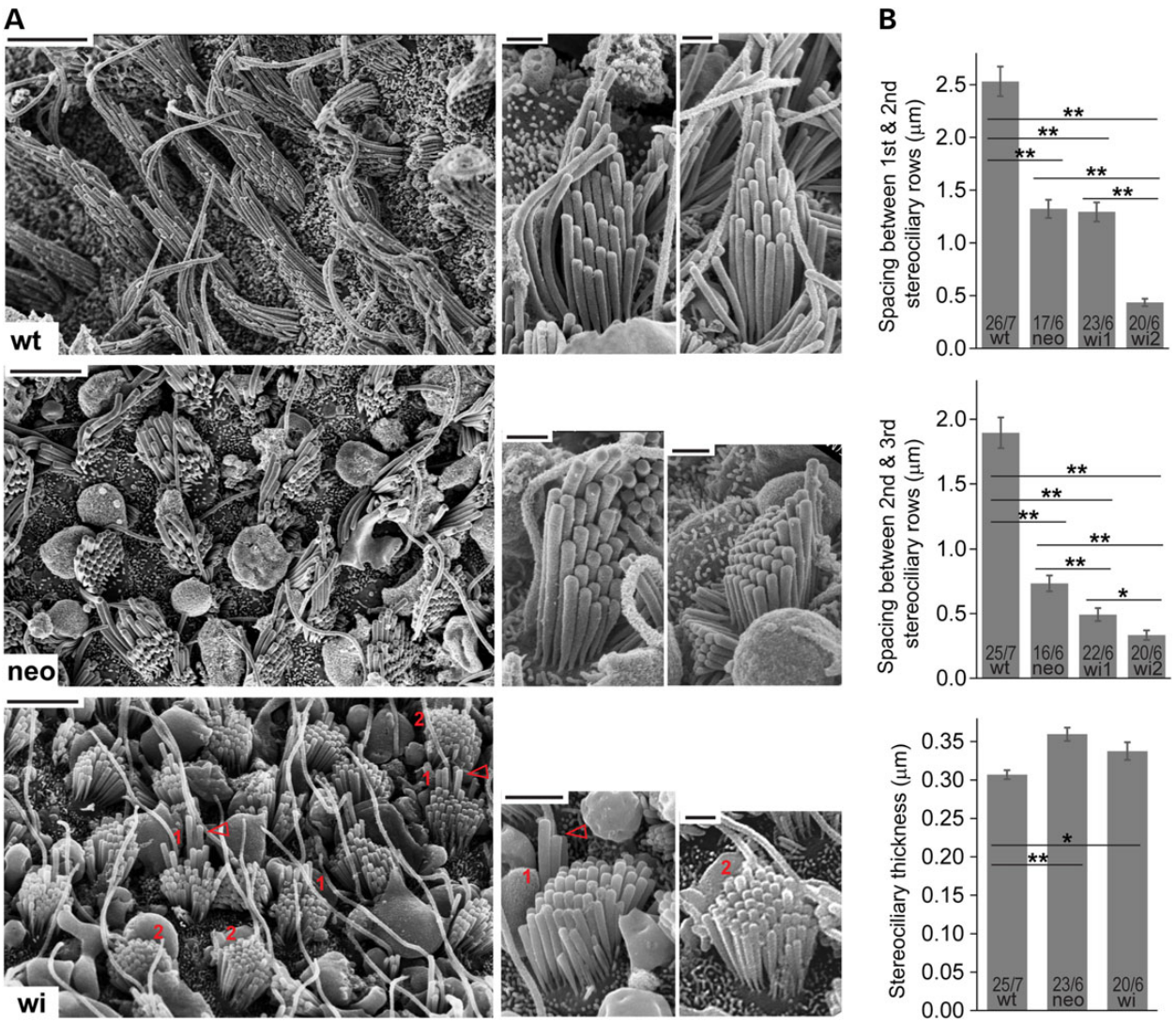

Figure 5. SEM observation of *Dfnb31*$^{neo/neo}$ and *Dfnb31*$^{wi/wi}$ vestibular stereociliary bundles. (**A**) Left, low-magnification images of the sensory epithelium from P45 wild-type (wt), *Dfnb31*$^{neo/neo}$ (neo) and *Dfnb31*$^{wi/wi}$ (wi) otolith organs. Stereociliary length is significantly reduced in *Dfnb31*$^{neo/neo}$ and *Dfnb31*$^{wi/wi}$ vestibular hair bundles, with *Dfnb31*$^{neo/neo}$ hair bundles being longer than *Dfnb31*$^{wi/wi}$ hair bundles. In general, *Dfnb31*$^{neo/neo}$ hair bundles have more obvious staircase arrangement of stereocilia than *Dfnb31*$^{wi/wi}$ hair bundles. However, there appears to be two types of *Dfnb31*$^{wi/wi}$ hair bundles. The *Dfnb31*$^{wi/wi}$ hair bundles labeled by '1' in red have relatively longer tallest stereocilia (red arrows) than the *Dfnb31*$^{wi/wi}$ hair bundles labeled by '2'. Scale bars, 5 μm. Right, representative single stereociliary bundles from wild-type, *Dfnb31*$^{neo/neo}$ and *Dfnb31*$^{wi/wi}$ otolith organs at P40–P45. Besides shorter stereocilia, the *Dfnb31*$^{neo/neo}$ and *Dfnb31*$^{wi/wi}$ vestibular hair bundles have thicker stereocilia. Scale bars, 1 μm. (**B**) Quantification of distance between stereociliary rows and stereociliary thickness. Top, the distances between the tallest and the second tallest stereociliary rows in *Dfnb31*$^{neo/neo}$ and *Dfnb31*$^{wi/wi}$ vestibular bundles are shorter than that in wild-types. Compared with *Dfnb31*$^{neo/neo}$ bundles, wi2 *Dfnb31*$^{wi/wi}$ bundles have a shorter distance and wi1 *Dfnb31*$^{wi/wi}$ bundles have a similar distance. Middle, the distances between the second and third tallest stereociliary rows in *Dfnb31*$^{neo/neo}$ and *Dfnb31*$^{wi/wi}$ vestibular bundles are shorter than that in wild-types, with *Dfnb31*$^{wi/wi}$ bundles having the shortest distance. Bottom, both *Dfnb31*$^{neo/neo}$ and *Dfnb31*$^{wi/wi}$ vestibular bundles have thicker stereocilia than wild-type bundles. Error bars, standard error of the mean; $^{**}P < 0.01$; $^{*}P < 0.05$.

Discussion

This study presents the first definitive evidence that various *Dfnb31* mutations are able to lead to vestibular dysfunction in mice, no matter whether these mutations cause hearing loss with or without retinal degeneration. This finding suggests the possibility that *DFNB31*-deficient patients may have some degree of bilateral vestibulopathy with DFNB31 patients being more severe than USH2D patients. Our study also demonstrates that FL- and C-whirlin deficiencies lead to significant shortening and widening of VHC stereocilia in mice, which may represent an underlying cause of the observed vestibular dysfunction.

Although both FL- and C-whirlins are essential for normal vestibular stereociliary length, our findings demonstrate that they may have slightly different roles. We show that both *Dfnb31*$^{neo/neo}$ and *Dfnb31*$^{wi/wi}$ VHCs have significantly shorter stereocilia than wild-types with *Dfnb31*$^{neo/neo}$ stereocilia being just slightly longer than *Dfnb31*$^{wi/wi}$ stereocilia in most sensory epithelia of the vestibular system, including the entire saccule, utricle and central zone of the crista (Fig. 4 and data not shown). Considering the disruption of FL-whirlin expression in both *Dfnb31*$^{neo/neo}$ and *Dfnb31*$^{wi/wi}$ VHCs and the expression of an intact C-whirlin in *Dfnb31*$^{neo/neo}$ VHCs (Figs 1B, C and 2), the above finding indicates that FL-whirlin but not C-whirlin plays a predominant role in stereociliary elongation in the majority of VHCs. On the other hand, C-whirlin appears more important for stereociliary elongation in the VHCs of the crista peripheral region, because the stereocilia in this region of *Dfnb31*$^{neo/neo}$ mice

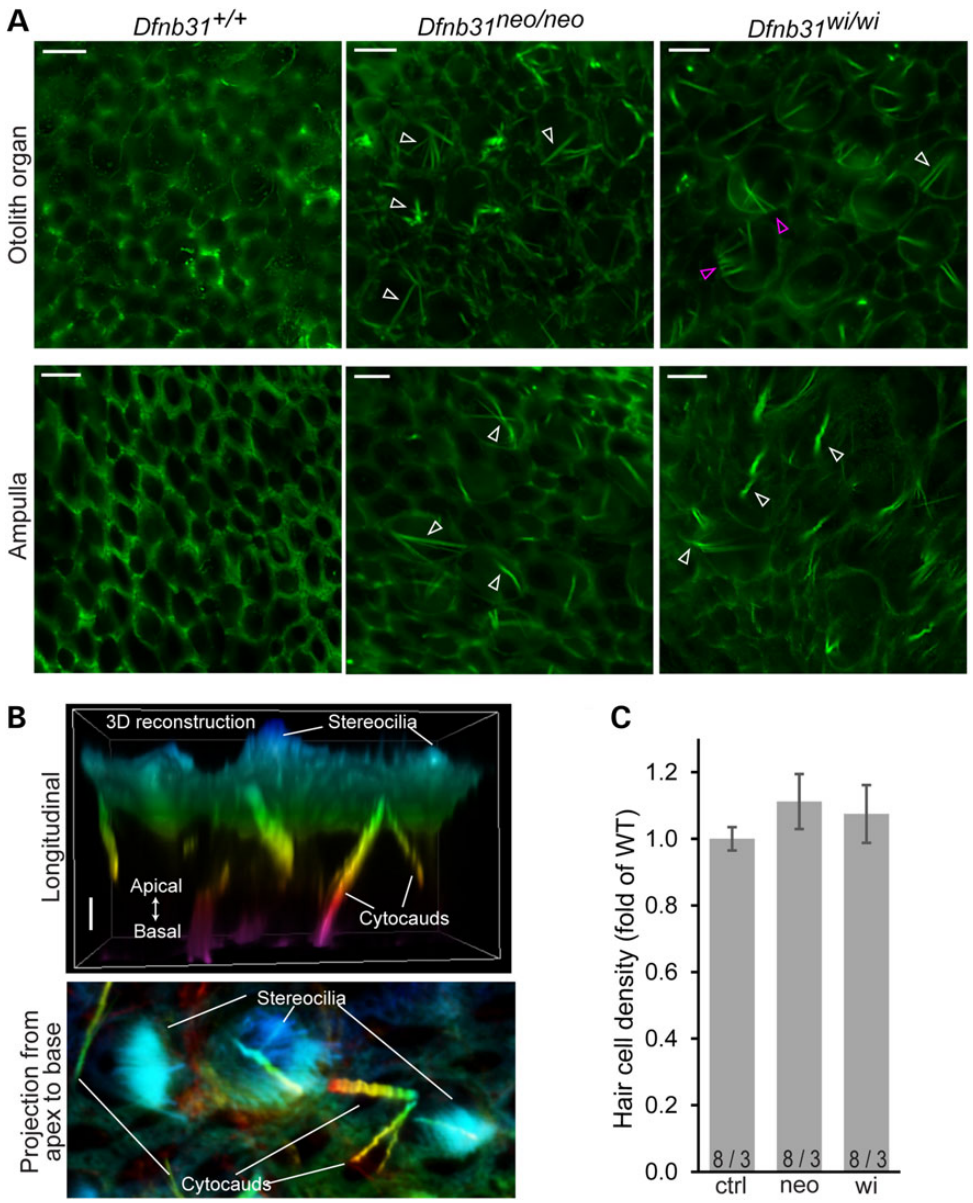

Figure 6. Cytocauds and hair cell densities in *Dfnb31*$^{neo/neo}$ and *Dfnb31*$^{wi/wi}$ vestibular organs. (**A**) Cytocauds (arrows) were revealed in *Dfnb31*$^{neo/neo}$ and *Dfnb31*$^{wi/wi}$ mice by staining otolith organs (upper row) and ampullae (lower row) for phalloidin at P4. Magenta arrows point to cytocauds originating from actin filaments at hair cell lateral surfaces. Images were taken at the level below the cuticular plate of hair cells. (**B**) Three-dimensional reconstruction of phalloidin signals from P4 *Dfnb31*$^{wi/wi}$ utricular hair cells. Upper, longitudinal view of phalloidin signals in the apical portion of hair cells. Lower, projection view of phalloidin signals along the apical–basal axis of hair cells. Phalloidin signals are pseudo-colored using a rainbow scale according to depth along hair cell apical–basal axis. Blue, apical; purple, basal. (**C**) Hair cell densities were analyzed in the striolar region of saccules from control (ctrl), *Dfnb31*$^{neo/neo}$ (neo) and *Dfnb31*$^{wi/wi}$ (wi) mice at P30. There was no significant difference among these genotype groups. Error bars are shown as standard error of the mean. Numbers before and after slashes are the numbers of saccular regions and mice examined, respectively. Student's *t* tests (two-tail) were performed. Scale bars, 5 μm in A and 1 μm in B.

are much longer than those of *Dfnb31*$^{wi/wi}$ mice (Figs. 2Ac and 3A and B). Additionally, C-whirlin may contribute to the formation of different lengths of stereociliary rows in the bundle, which is suggested by the existence of staircase-like stereociliary arrangement in *Dfnb31*$^{neo/neo}$ but not *Dfnb31*$^{wi/wi}$ VHCs (Figs. 2A, 4 and 5). Therefore, although the localization of whirlin isoforms in VHCs is similar to that of developing cochlear inner hair cells, the functional roles of the two whirlin isoforms appear not exactly the same in the two different types of hair cells. In the developing cochlear inner hair cells, C-whirlin is more important than FL-whirlin for normal stereociliary length (10). Furthermore, like in the cochlea (24,25), the change of stereociliary thickness occurs in *Dfnb31*$^{neo/neo}$ and *Dfnb31*$^{wi/wi}$ VHCs, suggesting that whirlin isoforms, especially FL-whirlin, also play a role in vestibular stereociliary thickness. This function could be contributed to by whirlin isoforms at both the stereociliary tip and the ankle link complex in VHCs.

To our knowledge, linear VsEP measurements of the present study represent the first direct testing of peripheral vestibular function in whirlin animal models. Our findings of severe to profound vestibular deficits from otolith organs of both *Dfnb31*$^{neo/neo}$ and *Dfnb31*$^{wi/wi}$ mice may be surprising, given the better performance of *Dfnb31*$^{neo/neo}$ mice in balance behavioral tests, especially

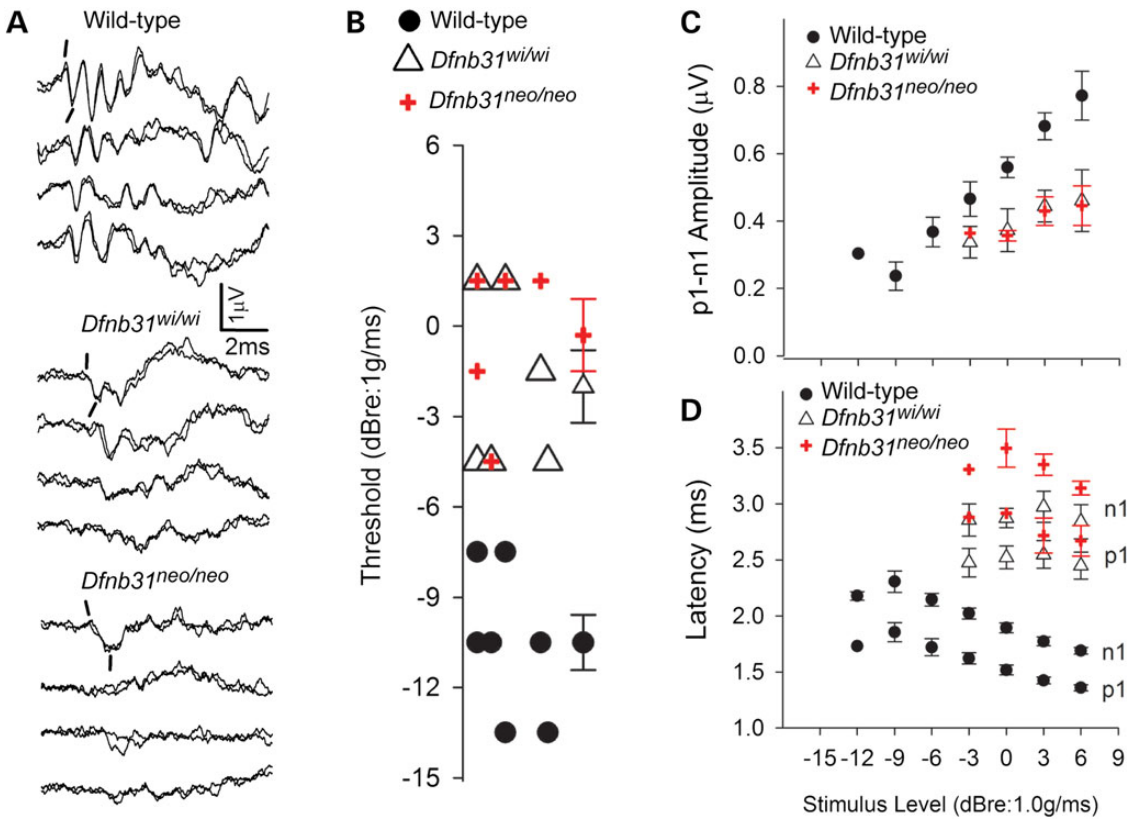

Figure 7. VsEP responses of *Dfnb31*$^{neo/neo}$ and *Dfnb31*$^{wi/wi}$ mice. (**A**) Representative VsEP responses from wild-type, *Dfnb31*$^{wi/wi}$ and *Dfnb31*$^{neo/neo}$ mutant mice. Prominent normal responses are present in wild-type animals, whereas responses are absent or appear as mere remnants of responses in the two mutant mouse groups. Positive peak p1 and negative peak n1 are marked for the first response pairs of each group. (**B**) VsEP threshold distributions are represented for all wild-type (filled circles) mice and for those mutant animals having responses (*Dfnb31*$^{wi/wi}$, open triangle, *Dfnb31*$^{neo/neo}$, plus sign). Mean and standard errors are shown to the right for each group. As can be seen there is no overlap between the distribution of wild-type and mutant genotypes, whereas the whirlin mutants have the same distribution. Mean thresholds for mutant mice were significantly higher than wild-types ($P < 5.0 \times 10^{-5}$). (**C** and **D**) VsEP response amplitudes (C, p1–n1) and latencies (D, p1, n1) as a function of stimulus level for wild-type (filled circles) and mutant mice (*Dfnb31*$^{wi/wi}$, open triangle, *Dfnb31*$^{neo/neo}$, plus sign). There was no overlap of the wild-type and mutant curves. Latencies were significantly prolonged for mutant animals (e.g. p1: $P < 6.0 \times 10^{-7}$) and amplitudes were significantly reduced (p1–n1, $P = 0.01$). Univariate ANOVA or MANOVA and *post hoc* tests with LSD were performed.

Table 1. Summary findings for VsEPs

	Threshold	p1	p1–n1
WT	−10.5 ± 2.45 (7)	1359 ± 72 (7)	0.77 ± 0.19 (7)
Dfnb31$^{wi/wi}$	−2.0 ± 2.9 (6)**	2448 ± 294 (6)***	0.46 ± 0.22 (6)*
Dfnb31$^{neo/neo}$	−0.3 ± 2.7 (5)**	2669 ± 304 (5)***	0.45 ± 0.13 (5)*

Threshold in dB re:1g/ms. p1 latency in μs and p1–n1 amplitude in μV at stimulus level of + 6 $dB_{re:1g/ms}$.
Comparisons made to wild-type (WT) animals: *$P = 0.01$, **$P < 5.0 \times 10^{-5}$, ***$P < 6.0 \times 10^{-7}$. *Post hoc* LSDs.

the swimming test, which significantly reduces proprioceptive compensation. Indeed, the balance behaviors tested in this study require some gravity receptor input to the central nervous system (CNS). The ability of the CNS to compensate for loss of vestibular function is remarkable and even the smallest residual function in many cases provides sufficient information to achieve relatively normal balance behaviors (33). The absence of the VsEP in a majority of *Dfnb31*$^{neo/neo}$ mice (64%) demonstrates that the level of synchronous neural input was exceedingly small, so small that the number of neurons firing synchronously in response to the stimulus was simply too few to be resolved by VsEP measurement. We have reported similar results in other mutants with profound vestibular loss (i.e. absent VsEP with absent or subtle defects in behavior and swimming tests, e.g. in 31). In contrast to the *Dfnb31*$^{neo/neo}$ mice, *Dfnb31*$^{wi/wi}$ animals circled, oriented abnormally in water and remained on the rotating rod for less time. This was true despite evidence of remnant gravity receptor responses in 50% of the *Dfnb31*$^{wi/wi}$ animals. Thus, in *Dfnb31*$^{wi/wi}$ mice, their behaviors indicated that the CNS was probably unable to compensate adequately for the incomplete peripheral loss, and that the dysfunction may extend to central motor control systems and/or to somatomotor reflex circuitry itself.

Evidence supporting a wider influence of whirlin on neural function outside of the inner ear and retina has been provided recently. Whirlin is expressed widely in the central and peripheral nervous system, including somatomotor reflex circuits and has been shown to be absent in these tissues of *Dfnb31*$^{wi/wi}$ mice (25,34,35). It is possible therefore that the complex circuitry supporting behaviors such as swimming is sufficiently compromised to contribute to the severe swimming and locomotor phenotype of the *Dfnb31*$^{wi/wi}$ mouse. A corollary to this hypothesis is that much of the central deficit must be rescued to some extent in the *Dfnb31*$^{neo/neo}$ mouse, since it can successfully orient in the water. This hypothesis requires that C-whirlin serves as a

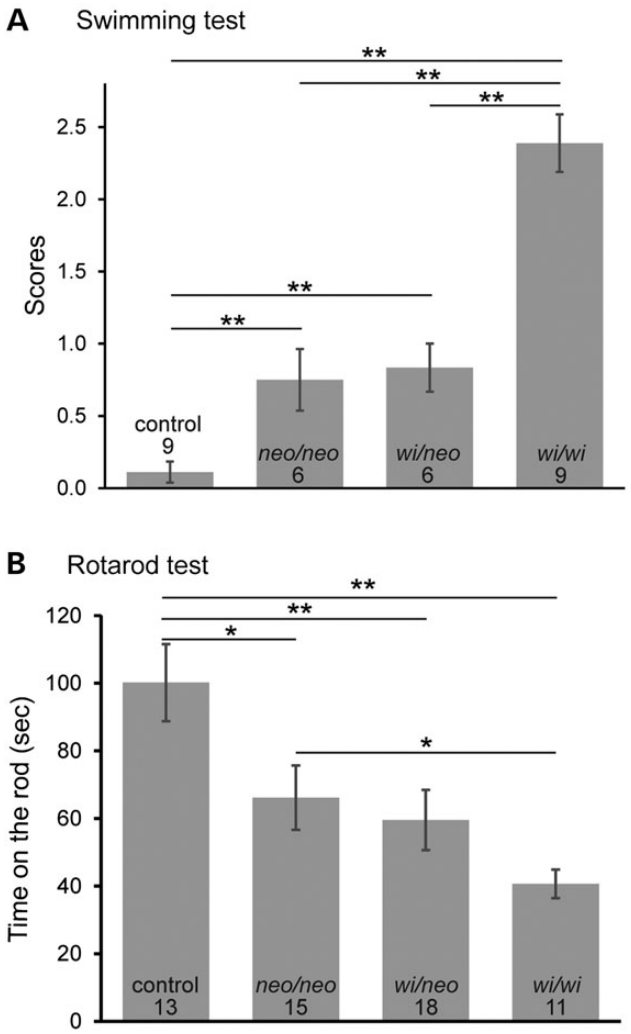

Figure 8. Balance behavioral tests on *Dfnb31*$^{neo/neo}$, *Dfnb31*$^{wi/neo}$ and *Dfnb31*$^{wi/wi}$ mice. (**A**) Swimming test scores of control, *Dfnb31*$^{neo/neo}$ (*neo/neo*), *Dfnb31*$^{wi/neo}$ (*wi/neo*) and *Dfnb31*$^{wi/wi}$ (*wi/wi*) mice at P60. *Dfnb31*$^{neo/neo}$ and *Dfnb31*$^{wi/neo}$ mice were able to swim better than *Dfnb31*$^{wi/wi}$ mice, while the *Dfnb31*$^{neo/neo}$ and *Dfnb31*$^{wi/neo}$ mice had similar swimming behaviors. All *Dfnb31* mutant mice had abnormal swimming behaviors, compared with control mice. Swimming test scores were defined as follows (32): 0, normal swimming; 1, irregular swimming; 2, immobile floating; and 3, underwater tumbling. (**B**) Rotarod test results of control, *Dfnb31*$^{neo/neo}$, *Dfnb31*$^{neo/wi}$ and *Dfnb31*$^{wi/wi}$ mice at P35–45. *Dfnb31*$^{neo/neo}$, *Dfnb31*$^{wi/neo}$ and *Dfnb31*$^{wi/wi}$ mice could not stay on the rotating rod as long as control mice. *Dfnb31*$^{neo/neo}$ and *Dfnb31*$^{wi/neo}$ mice performed better than *Dfnb31*$^{wi/wi}$ mice, while *Dfnb31*$^{neo/neo}$ and *Dfnb31*$^{neo/wi}$ mice had similar levels of performance. Error bars are shown as standard error of the mean. Numbers at the bottom of each bar are numbers of mice tested. Student's *t*-tests (two-tail) were performed. $^{**}P < 0.01$; $^{*}P < 0.05$.

functional replacement for FL-whirlin and partially restores function in neural elements outside of the inner ear and retina.

Another factor that may contribute to better balance behaviors of *Dfnb31*$^{neo/neo}$ mice despite their linear VsEP abnormality similar to *Dfnb31*$^{wi/wi}$ mice is the potential better semicircular canal function of *Dfnb31*$^{neo/neo}$ mice. In the vestibular system, otolith organs are responsible for linear acceleration and gravity sensation, and semicircular canals sense angular acceleration. It has been shown that mice with defective otolith organs, such as *Nox3*, *Otop1*, *Muted* and *Cyba* mice with absent otoconia, do not exhibit circling behaviors (36–39), whereas mice with horizontal semicircular canal problems tend to circle (40,41). We found *Dfnb31*$^{neo/neo}$ mice have much longer VHC stereocilia in the peripheral zone of the crista than *Dfnb31*$^{wi/wi}$ mice, suggesting the possibility that *Dfnb31*$^{neo/neo}$ mice have better semicircular canal function. This could explain the absence and presence of a circling behavior of *Dfnb31*$^{neo/neo}$ and *Dfnb31*$^{wi/wi}$ mice, respectively, despite these two mutants having similar levels of macular dysfunction. The better stereociliary morphology in *Dfnb31*$^{neo/neo}$ cristae may also explain the better rotarod performance of this *Dfnb31* mutant mouse. On the other hand, better semicircular canal function is not likely to explain the improved swimming behavior (i.e. ability to orient and consistently reach the water surface) in *Dfnb31*$^{neo/neo}$ mice, inasmuch as normal semicircular canal function in otoconia-deficient mice does not rescue abnormal swimming behaviors (36–39,42).

DFNB31 mutations have been shown to cause USH2D (1–3), non-syndromic deafness DFNB31 (4,5) and non-syndromic retinal degeneration (6). All of these diseases are characterized by normal vestibular function in human patients. This raises the question of whether the absence of evidence for vestibular dysfunction in the human reflects a real species difference in the consequences of *DFNB31*/*Dfnb31* mutations? Or is there an occult macular deficit in the human that is masked as a result of CNS compensation to peripheral sensory weakness or alternatively a deficit unseen due to a limitation of the assessment methods available for testing human macular function; or perhaps both?

USH2D patients are thought to represent a small fraction of the USH2 patient population as a whole (43). Investigations providing in-depth vestibular, balance and posturography testing of USH2 patients to date have evaluated a relatively small number of subjects [e.g. $n = 9$, (44)]. Although they reported no vestibular deficits in USH2 patients, it is possible that the small sample did not include USH2D patients since genotyping was not possible at that time. Overall, only a limited number of confirmed USH2D patients have been studied (1–3). In most of these cases, no direct measurements of vestibular function were made. Objective vestibular testing was reported in the study of one family which defined USH2D for the first time (3). Testing consisted of recording the medical history of motor development and measuring the response to caloric stimulation. The findings consistently indicated normal vestibular function in USH2D patients. Similarly, only one study examined DFNB31 patients from one family for vestibular dysfunction and concluded normal vestibular function (5), although the details of vestibular function measurement were not given. In fact, a recent survey-based study on patients with non-syndromic deafness DFNB1 shows that 54% of 235 patients may have vestibular dysfunction (45). Therefore, it is possible that in *DFNB31*-deficient patients, a more moderate vestibular macular deficit existed and hypothetically was not apparent as a result of CNS compensation and/or because the tests used were insensitive to macular deficits (e.g. caloric tests). This is a question that may be addressed in the future using more sensitive clinical tests now available including cervical and ocular vestibular-evoked myogenic potentials or off-axis rotational tests. Clarifying these issues will be important if we are to fully understand the mechanisms at work in the development of *DFNB31*/*Dfnb31*-related diseases in both humans and mice.

In summary, our molecular, morphological, direct functional and behavioral studies on the vestibular system of whirlin mutant mice demonstrate that the expression and localization of FL- and C-whirlins in VHCs are similar to those found in developing cochlear inner hair cells with both whirlins at stereociliary tips and only FL-whirlin at the ankle link complex. Both FL- and C-whirlin proteins are indispensable for normal vestibular

stereociliary dimensions, macular neuroepithelial function and balance behaviors.

Materials and Methods

Animals

Dfnb31 targeted mutant (*Dfnb31*$^{neo/neo}$ also known as *Dfnb31*^{tm1Tili}, MGI:4462398) and whirler (*Dfnb31*$^{wi/wi}$, MGI:1857090) mice were described previously (4,7). *Dfnb31*$^{wi/neo}$ mice were generated by crossing *Dfnb31*$^{neo/neo}$ and *Dfnb31*$^{wi/wi}$ mice. *Dfnb31*$^{tm1a(EUCOMM)wtsi}$ mice (MGI:4432119) were purchased as frozen sperms from EUCOMM and revived at the University of Utah Transgenic and Gene Targeting mouse core. All experiments involving animals were performed in compliance with the Institutional Animal Care and Use Committees at the University of Utah and the University of Nebraska-Lincoln.

Antibodies and reagents

Two His tag-fused whirlin fragments (1–124 aa and 375–800 aa, NP_082916, in pET28 vector) were expressed in BL21-CodonPlus (DE3)-RIPL cells (Agilent Technologies, Santa Clara, CA, USA), and purified by chromatography using Ni^{2+}-charged His•Bind resin (EMD Millipore, Billerica, MA, USA). Two GST-fused whirlin fragments (1–472 aa and 721–907 aa, NP_082916, in pGEX-4T-1 vector) were expressed in the same BL21 cells as above, and purified by chromatography using glutathione sepharose™ 4 Fast Flow resin (GE Healthcare Life Sciences, Pittsburgh, PA, USA). The purified His-tagged whirlin proteins were used to immunize rabbits, and antibodies against whirlin were affinity-purified against the corresponding GST-tagged whirlin fragments. The specificity of the purified antibodies was confirmed by immunoblotting of recombinant whirlin N- and C-terminal fragments expressed in HEK293 cells (data not shown). Antibodies against calretinin, β-III tubulin (TUJ1) and oncomodulin were purchased from Millipore (Temecula, CA, USA), Covance (Princeton, NJ, USA) and Santa Cruz Biotechnology (Dallas, TX, USA), respectively. Alexa fluorochrome-conjugated phalloidin and secondary antibodies were obtained from Life Technologies (Grand Island, NY, USA).

RNA isolation and RT–PCR

Total RNA was extracted from P4 mouse vestibular organs using SurePrep™ RNA Purification Kit (Fisher BioReagents®, Fair Lawn, NJ, USA). RT–PCR was conducted from total RNA using Thermoscript RT–PCR kit (Life Technologies) and Expand Long Template PCR System (Roche Life Science, Indianapolis, IN, USA). Manufacturer's instructions were followed exactly during RNA isolation and RT–PCR.

Immunofluorescence, 3D reconstruction and SEM

Procedures for immunofluorescence of mouse vestibular tissues were the same as previously reported (16). Fluorescent images were taken using a confocal laser scanning microscope (Model FV1000, Olympus, Tokyo, Japan). To build the 3D reconstruction of confocal images, a series of images taken at a 0.2-μm step along the z-axis were first deconvoluted using Autoquant ×3 (Bitplane, South Windsor, CT, USA) and then reconstructed using Elements software from Nikon (Melville, NY, USA). Z-dimensional data were converted to lambda and coded by pseudocolor. First and last stacks were assigned to the two end wavelengths of rainbow, while middle stacks obtained wavelength values in between. SEM procedures were described previously (16).

Measurements of vestibular stereociliary length, thickness, distance between stereociliary rows and hair cell density

All measurements were performed blind to genotype using ImageJ. Stereociliary length of the vestibular system was measured in confocal images of phalloidin-stained whole-mounts. Measurements were performed on the longest stereocilia in the bundle exclusively in the central region of cristae and mostly in the extrastriolar region of saccules. Stereociliary thickness and distance between stereociliary rows were assessed using SEM images of mouse otolith organs. For the stereociliary thickness, two stereocilia in the tallest row of one bundle were measured and averaged. The distance between the tallest and the second tallest rows as well as the distance between the second and third tallest rows were measured in hair bundles with discernable stereociliary rows. To calculate the hair cell density, total numbers of hair bundles within an area of 1778 μm^2 were counted at the saccular striola. The hair cell densities of whirlin mutant mice were normalized by the hair cell density of wild-type mice.

Swimming and rotarod tests

For swimming tests, mice were placed in a large container filled with warm water. Their swimming behaviors were observed blind to genotype. Scores of 0–3 were assigned according to the criteria published previously (32). In short, a score of 0 denoted normal swimming behaviors, while scores of increasing numbers indicated an increasing severity of abnormal swimming behaviors with a score of 3 being underwater tumbling. Rotarod tests were performed on adult mice using a ROTO-ROD Series 8 machine (IITC Life Science, Woodland Hills, CA, USA) over a period of 3 consecutive days. Mice were trained the first 2 days and tested on the third day during the same time period of the day to eliminate a circadian behavioral difference. Before any trials each day, mice were maintained in the test room for at least 30 min to adapt to the environment. Five trials per day were conducted. During each trial, mice were kept on a rotating rod for a maximum period of 180 s or until they fell. The rotating rod started at a speed of 5 rpm, increased to 10 rpm in 120 s, and remained at 10 rpm on day 1. The rotating speed was then changed to 7 rpm at the beginning, accelerated to 15 rpm in 120 s and kept at 15 rpm on day 2. On day 3, the rotating rod was initiated at 15 rpm and accelerated to 25 rpm in 120 s. Between the five trials on the same day, mice were given a 5 min rest with free access to food and water. On day 3, the lengths of time mice were able to stay on the rotating rod were recorded and averaged from the five trials of the same mice.

Vestibular sensory-evoked potential

The linear VsEP is a compound action potential produced by eighth nerve neurons innervating gravity receptors (otolith organs) and their central relays in the brainstem (33,46–48). During VsEP testing, mice were deeply anesthetized by intraperitoneal injection of ketamine/xylazine (18:2 mg/ml; 5–7 μl/g body weight) followed by maintenance doses of 0.05 ml every 60 min as needed to maintain adequate anesthesia. Core body temperature was maintained at 37.0 ± 0.2°C using a homeothermic heating blanket system.

VsEP recordings were based on methods published previously (46,48,49). Briefly, vestibular stimuli (linear head translations) were delivered by securing the mouse head to a mechanical shaker (Model ET-132203, Labworks Inc., Costa Mesa, CA, USA) using a non-invasive head clip. Linear acceleration ramps (17 pulses/s, 2 ms duration) were used to generate rectangular (step) jerk stimuli specified in units of g/ms, where 1 g = 9.8 m/s^2, that were in turn applied to the head. Jerk stimuli ranged in amplitude from + 6 to −18dBre:1 g/ms and were adjusted in levels of 3 dB. Stimuli were presented to the head in the naso-occipital axis, thus stimulating both saccular and utricular receptors.

Subcutaneous needle electrodes were placed posterior to the right pinna and at the right hip for inverting and ground electrodes, respectively. Stainless-steel wire placed subcutaneously at the nuchal crest served as the non-inverting electrode. Electroencephalographic activity was amplified (×200 000), filtered (300–3000 Hz) and digitized (1024 points at 10 μs/point). Two hundred and fifty-six primary responses were averaged and replicated for each VsEP waveform. A VsEP intensity series was collected beginning at the maximum stimulus level (i.e. +6 dB re: 1.0 g/ms) with and without acoustic masking (50–50 000 Hz forward masker at 90 dB SPL), and then stimulus levels were increased from −18 dB to +6 dBre:1 g/ms in 3 dB steps to determine vestibular response threshold. Threshold was defined as the stimulus level halfway between the highest level failing to produce a response and the lowest level producing a response.

The first two VsEP positive (p1) and negative (n1) response peaks were scored. Latency was defined as the elapsed time from the stimulus onset to the scored response peak (μs). Response amplitudes were defined as the amplitude of the positive peak (in microvolts) minus the amplitude of the negative peak (p1–n1). These provided response measures for vestibular peripheral nerve response onset latencies and amplitudes (47). These response metrics as well as threshold were used to evaluate the effects of genotype.

Statistics

Student's *t*-tests were conducted using Microsoft Office Excel to compare the following values between two genotype groups: stereociliary lengths, stereociliary thicknesses, distances between stereociliary rows, cell densities, swimming scores and times remaining on Rotarod. A *P*-value of <0.05 was considered to indicate a statistically significant difference between groups. For VsEP data, univariate ANOVA or MANOVA (SPSS v.22, Chicago, IL, USA) was used to compare latencies, amplitudes and thresholds between genotypes and LSD was used for *post hoc* tests.

Supplementary Material

Supplementary Material is available at *HMG* online.

Acknowledgements

We thank the Wellcome Trust Sanger Institute Mouse Genetics Project (Sanger MGP) and its funders for providing the mutant mouse line (Allele: *Dfnb31*$^{tm1a(EUCOMM)wtsi}$).

Conflict of Interest statement. None declared.

Funding

This work was supported by the National Institutes of Health (EY020853 to J.Y., EY014800 to the Department of Ophthalmology and Visual Sciences, University of Utah); Research to Prevent Blindness, Inc. (to J.Y. and the Department of Ophthalmology and Visual Sciences, University of Utah); Hearing Health Foundation; the Nebraska Tobacco Settlement Biomedical Research Foundation (T.A.J, S.M.J.); Department of Special Education and Communication Disorders, UNL (T.A.J., S.V.) and a startup package from the Moran Eye Center, University of Utah (to J.Y.).

References

1. Audo, I., Bujakowska, K., Mohand-Said, S., Tronche, S., Lancelot, M.E., Antonio, A., Germain, A., Lonjou, C., Carpentier, W., Sahel, J.A. *et al.* (2011) A novel DFNB31 mutation associated with Usher type 2 syndrome showing variable degrees of auditory loss in a consanguineous Portuguese family. *Mol. Vis.*, **17**, 1598–1606.
2. Besnard, T., Vache, C., Baux, D., Larrieu, L., Abadie, C., Blanchet, C., Odent, S., Blanchet, P., Calvas, P., Hamel, C. *et al.* (2012) Non-USH2A mutations in USH2 patients. *Hum. Mutat.*, **33**, 504–510.
3. Ebermann, I., Scholl, H.P., Charbel Issa, P., Becirovic, E., Lamprecht, J., Jurklies, B., Millan, J.M., Aller, E., Mitter, D. and Bolz, H. (2007) A novel gene for Usher syndrome type 2: mutations in the long isoform of whirlin are associated with retinitis pigmentosa and sensorineural hearing loss. *Hum. Genet.*, **121**, 203–211.
4. Mburu, P., Mustapha, M., Varela, A., Weil, D., El-Amraoui, A., Holme, R.H., Rump, A., Hardisty, R.E., Blanchard, S., Coimbra, R.S. *et al.* (2003) Defects in whirlin, a PDZ domain molecule involved in stereocilia elongation, cause deafness in the whirler mouse and families with DFNB31. *Nat. Genet.*, **34**, 421–428.
5. Tlili, A., Charfedine, I., Lahmar, I., Benzina, Z., Mohamed, B.A., Weil, D., Idriss, N., Drira, M., Masmoudi, S. and Ayadi, H. (2005) Identification of a novel frameshift mutation in the DFNB31/WHRN gene in a Tunisian consanguineous family with hereditary non-syndromic recessive hearing loss. *Hum. Mutat.*, **25**, 503–507.
6. Nishiguchi, K.M., Tearle, R.G., Liu, Y.P., Oh, E.C., Miyake, N., Benaglio, P., Harper, S., Koskiniemi-Kuendig, H., Venturini, G., Sharon, D. *et al.* (2013) Whole genome sequencing in patients with retinitis pigmentosa reveals pathogenic DNA structural changes and NEK2 as a new disease gene. *Proc. Natl Acad. Sci. USA*, **110**, 16139–16144.
7. Yang, J., Liu, X., Zhao, Y., Adamian, M., Pawlyk, B., Sun, X., McMillan, D.R., Liberman, M.C. and Li, T. (2010) Ablation of whirlin long isoform disrupts the USH2 protein complex and causes vision and hearing loss. *PLoS Genet.*, **6**, e1000955.
8. Wright, R.N., Hong, D.H. and Perkins, B. (2012) RpgrORF15 connects to the usher protein network through direct interactions with multiple whirlin isoforms. *Invest. Ophthalmol. Vis. Sci.*, **53**, 1519–1529.
9. Kikkawa, Y., Mburu, P., Morse, S., Kominami, R., Townsend, S. and Brown, S.D. (2005) Mutant analysis reveals whirlin as a dynamic organizer in the growing hair cell stereocilium. *Hum. Mol. Genet.*, **14**, 391–400.
10. Mathur, P., Zou, J., Zheng, T., Almishaal, A., Wang, Y., Chen, Q., Wang, L., Vashist, D., Brown, S., Park, A. *et al.* (2015) Distinct expression and function of whirlin isoforms in the inner ear and retina: an insight into pathogenesis of USH2D and DFNB31. *Hum. Mol. Genet.*, **24**, 6213–6228.
11. Holme, R.H., Kiernan, B.W., Brown, S.D. and Steel, K.P. (2002) Elongation of hair cell stereocilia is defective in the mouse mutant whirler. *J. Comp. Neurol.*, **450**, 94–102.

12. Chen, Q., Zou, J., Shen, Z., Zhang, W. and Yang, J. (2014) Whirlin and PDZ domain containing 7 (PDZD7) proteins are both required to form the quaternary protein complex associated with Usher syndrome type 2. *J. Biol. Chem.*, **289**, 36070–36088.
13. Michalski, N., Michel, V., Bahloul, A., Lefevre, G., Barral, J., Yagi, H., Chardenoux, S., Weil, D., Martin, P., Hardelin, J.P. *et al.* (2007) Molecular characterization of the ankle-link complex in cochlear hair cells and its role in the hair bundle functioning. *J. Neurosci.*, **27**, 6478–6488.
14. Goodyear, R.J., Marcotti, W., Kros, C.J. and Richardson, G.P. (2005) Development and properties of stereociliary link types in hair cells of the mouse cochlea. *J. Comp. Neurol.*, **485**, 75–85.
15. Grati, M., Shin, J.B., Weston, M.D., Green, J., Bhat, M.A., Gillespie, P.G. and Kachar, B. (2012) Localization of PDZD7 to the stereocilia ankle-link associates this scaffolding protein with the Usher syndrome protein network. *J. Neurosci.*, **32**, 14288–14293.
16. Zou, J., Zheng, T., Ren, C., Askew, C., Liu, X.P., Pan, B., Holt, J.R., Wang, Y. and Yang, J. (2014) Deletion of PDZD7 disrupts the Usher syndrome type 2 protein complex in cochlear hair cells and causes hearing loss in mice. *Hum. Mol. Genet.*, **23**, 2374–2390.
17. Belyantseva, I.A., Boger, E.T., Naz, S., Frolenkov, G.I., Sellers, J.R., Ahmed, Z.M., Griffith, A.J. and Friedman, T.B. (2005) Myosin-XVa is required for tip localization of whirlin and differential elongation of hair-cell stereocilia. *Nat. Cell Biol.*, **7**, 148–156.
18. Delprat, B., Michel, V., Goodyear, R., Yamasaki, Y., Michalski, N., El-Amraoui, A., Perfettini, I., Legrain, P., Richardson, G., Hardelin, J.P. *et al.* (2005) Myosin XVa and whirlin, two deafness gene products required for hair bundle growth, are located at the stereocilia tips and interact directly. *Hum. Mol. Genet.*, **14**, 401–410.
19. Fleming, J., Rogers, M.J., Brown, S.D. and Steel, K.P. (1994) Linkage analysis of the whirler deafness gene on mouse chromosome 4. *Genomics*, **21**, 42–48.
20. Simmons, D.D., Tong, B., Schrader, A.D. and Hornak, A.J. (2010) Oncomodulin identifies different hair cell types in the mammalian inner ear. *J. Comp. Neurol.*, **518**, 3785–3802.
21. Desai, S.S., Zeh, C. and Lysakowski, A. (2005) Comparative morphology of rodent vestibular periphery. I. Saccular and utricular maculae. *J. Neurophysiol.*, **93**, 251–266.
22. Li, A., Xue, J. and Peterson, E.H. (2008) Architecture of the mouse utricle: macular organization and hair bundle heights. *J. Neurophysiol.*, **99**, 718–733.
23. Pujol, R., Pickett, S.B., Nguyen, T.B. and Stone, J.S. (2014) Large basolateral processes on type II hair cells comprise a novel processing unit in mammalian vestibular organs. *J. Comp. Neurol.*, **522**, 3141–3159.
24. Mogensen, M.M., Rzadzinska, A. and Steel, K.P. (2007) The deaf mouse mutant whirler suggests a role for whirlin in actin filament dynamics and stereocilia development. *Cell Motil. Cytoskeleton*, **64**, 496–508.
25. Wang, L., Zou, J., Shen, Z., Song, E. and Yang, J. (2012) Whirlin interacts with espin and modulates its actin-regulatory function: an insight into the mechanism of Usher syndrome type II. *Hum. Mol. Genet.*, **21**, 692–710.
26. Anniko, M., Sobin, A. and Wersall, J. (1980) Vestibular hair cell pathology in the Shaker-2 mouse. *Arch. Otorhinolaryngol.*, **226**, 45–50.
27. Probst, F.J., Fridell, R.A., Raphael, Y., Saunders, T.L., Wang, A., Liang, Y., Morell, R.J., Touchman, J.W., Lyons, R.H., Noben-Trauth, K. *et al.* (1998) Correction of deafness in shaker-2 mice by an unconventional myosin in a BAC transgene. *Science*, **280**, 1444–1447.
28. Beyer, L.A., Odeh, H., Probst, F.J., Lambert, E.H., Dolan, D.F., Camper, S.A., Kohrman, D.C. and Raphael, Y. (2000) Hair cells in the inner ear of the pirouette and shaker 2 mutant mice. *J. Neurocytol.*, **29**, 227–240.
29. Kanzaki, S., Beyer, L.A., Canlon, B., Meixner, W.M. and Raphael, Y. (2002) The cytocaud: a hair cell pathology in the waltzing Guinea pig. *Audiol. Neurootol.*, **7**, 289–297.
30. Mustapha, M., Beyer, L.A., Izumikawa, M., Swiderski, D.L., Dolan, D.F., Raphael, Y. and Camper, S.A. (2007) Whirler mutant hair cells have less severe pathology than shaker 2 or double mutants. *J. Assoc. Res. Otolaryngol.*, **8**, 329–337.
31. Goodyear, R.J., Jones, S.M., Sharifi, L., Forge, A. and Richardson, G.P. (2012) Hair bundle defects and loss of function in the vestibular end organs of mice lacking the receptor-like inositol lipid phosphatase PTPRQ. *J. Neurosci.*, **32**, 2762–2772.
32. Hardisty-Hughes, R.E., Parker, A. and Brown, S.D. (2010) A hearing and vestibular phenotyping pipeline to identify mouse mutants with hearing impairment. *Nat. Protoc.*, **5**, 177–190.
33. Jones, S.M. and Jones, T.A. (2014) Genetics of peripheral vestibular dysfunction: lessons from mutant mouse strains. *J. Am. Acad. Audiol.*, **25**, 289–301.
34. Yap, C.C., Liang, F., Yamazaki, Y., Muto, Y., Kishida, H., Hayashida, T., Hashikawa, T. and Yano, R. (2003) CIP98, a novel PDZ domain protein, is expressed in the central nervous system and interacts with calmodulin-dependent serine kinase. *J. Neurochem.*, **85**, 123–134.
35. Green, J.A., Yang, J., Grati, M., Kachar, B. and Bhat, M.A. (2013) Whirlin, a cytoskeletal scaffolding protein, stabilizes the paranodal region and axonal cytoskeleton in myelinated axons. *BMC Neurosci.*, **14**, 96.
36. Nakano, Y., Longo-Guess, C.M., Bergstrom, D.E., Nauseef, W.M., Jones, S.M. and Banfi, B. (2008) Mutation of the Cyba gene encoding p22phox causes vestibular and immune defects in mice. *J. Clin. Invest.*, **118**, 1176–1185.
37. Lyon, M.F. (1951) Hereditary absence of otoliths in the house mouse. *J. Physiol.*, **114**, 410–418.
38. Paffenholz, R., Bergstrom, R.A., Pasutto, F., Wabnitz, P., Munroe, R.J., Jagla, W., Heinzmann, U., Marquardt, A., Bareiss, A., Laufs, J. *et al.* (2004) Vestibular defects in head-tilt mice result from mutations in Nox3, encoding an NADPH oxidase. *Genes Dev.*, **18**, 486–491.
39. Hurle, B., Ignatova, E., Massironi, S.M., Mashimo, T., Rios, X., Thalmann, I., Thalmann, R. and Ornitz, D.M. (2003) Non-syndromic vestibular disorder with otoconial agenesis in tilted/mergulhador mice caused by mutations in otopetrin 1. *Hum. Mol. Genet.*, **12**, 777–789.
40. Jen, J.C. (2009) Bilateral vestibulopathy: clinical, diagnostic, and genetic considerations. *Semin. Neurol.*, **29**, 528–533.
41. Cryns, K., van Alphen, A.M., van Spaendonck, M.P., van de Heyning, P.H., Timmermans, J.P., de Zeeuw, C.I. and van Camp, G. (2004) Circling behavior in the Ecl mouse is caused by lateral semicircular canal defects. *J. Comp. Neurol.*, **468**, 587–595.
42. Zhao, X., Jones, S.M., Yamoah, E.N. and Lundberg, Y.W. (2008) Otoconin-90 deletion leads to imbalance but normal hearing: a comparison with other otoconia mutants. *Neuroscience*, **153**, 289–299.
43. Mathur, P. and Yang, J. (2015) Usher syndrome: hearing loss, retinal degeneration and associated abnormalities. *Biochim. Biophys. Acta*, **1852**, 406–420.
44. Moller, C.G., Kimberling, W.J., Davenport, S.L., Priluck, I., White, V., Biscone-Halterman, K., Odkvist, L.M., Brookhouser,

P.E., Lund, G. and Grissom, T.J. (1989) Usher syndrome: an otoneurologic study. *Laryngoscope*, **99**, 73–79.
45. Dodson, K.M., Blanton, S.H., Welch, K.O., Norris, V.W., Nuzzo, R.L., Wegelin, J.A., Marin, R.S., Nance, W.E., Pandya, A. and Arnos, K.S. (2011) Vestibular dysfunction in DFNB1 deafness. *Am. J. Med. Genet. A*, **155A**, 993–1000.
46. Jones, T.A. and Jones, S.M. (1999) Short latency compound action potentials from mammalian gravity receptor organs. *Hear. Res.*, **136**, 75–85.
47. Nazareth, A.M. and Jones, T.A. (1998) Central and peripheral components of short latency vestibular responses in the chicken. *J. Vestib. Res.*, **8**, 233–252.
48. Jones, S.M., Erway, L.C., Johnson, K.R., Yu, H. and Jones, T.A. (2004) Gravity receptor function in mice with graded otoconial deficiencies. *Hear. Res.*, **191**, 34–40.
49. Mock, B., Jones, T.A. and Jones, S.M. (2011) Gravity receptor aging in the CBA/CaJ strain: a comparison to auditory aging. *J. Assoc. Res. Otolaryngol.*, **12**, 173–183.